Synthesis and Spectroscopic Characterization of Fluorophore-Labeled Oligospiroketal Rods

by **Anne Techen**[a]), **Sylvia Czapla**[b]), **Kristian Möllnitz**[b]), **Dennis Budach**[b]), **Pablo Wessig***[b]), and **Michael U. Kumke***[a])

[a]) Universität Potsdam, Institut für Chemie, Physical Chemistry, Karl-Liebknecht-Strasse 24 – 25, D-14476 Potsdam (e-mail: kumke@uni-potsdam.de)

[b]) Universität Potsdam, Institut für Chemie, Bioorganic Chemistry, Karl-Liebknecht-Strasse 24 – 25, D-14476 Potsdam (e-mail: wessig@uni-potsdam.de)

Fluorescence probes consisting of well-established fluorophores in combination with rigid molecular rods based on spirane-type structures were investigated with respect to their fluorescence properties under different solvent conditions. The attachment of the dyes was accomplished by 1,3-dipolar cycloaddition between alkynes and azides ('*click*' *reaction*) and is a prime example for a novel class of sensor constructs. Especially, the attachment of two (different) fluorophores on opposite sides of the molecular rods paves the way to new sensor systems with less bulky (compared to the conventional DNA- or protein-based concepts), nevertheless rigid spacer constructs, *e.g.*, for FRET-based sensing applications. A detailed photophysical characterization was performed in MeOH (and in basic H_2O/MeOH mixtures) for *i*) rod constructs containing carboxyfluorescein, *ii*) rod constructs containing carboxyrhodamine, *iii*) rod constructs containing both carboxyfluorescein and carboxyrhodamine, and *iv*) rod constructs containing both pyrene and perylene parts. For each dye (pair), two rod lengths with different numbers of spirane units were synthesized and investigated. The rod constructs were characterized in ensemble as well as single-molecule fluorescence experiments with respect to *i*) specific rod–dye and *ii*) dye–dye interactions. In addition to MeOH and MeOH/NaOH, the rod constructs were also investigated in micellar systems, which were chosen as a simplified model for membranes.

Introduction. – In fluorescence-based applications, improved sensor dyes are needed steadily. Especially, the sensing of distances on the sub-nm scale using *Förster* resonance energy transfer (FRET) as the fundamental principle calls for novel, tailor-made fluorescence systems.

Specific interactions between the dye molecule and biochemical spacers such as DNA or polypeptides can be *i*) intercalation into the major grove of the DNA, *ii*) specific interaction with a nucleic acids or amino acids, *iii*) incorporation into polypeptides upon formation of the ternary structure, and many more [1]. Compared to conventional biochemical spacers, the oligospiroketal (OSK) rod [2] (see *Scheme 1*) is an attractive alternative, because *i*) the OSK rod is much smaller in diameter, making it less bulky and subsequently more suitable for incorporation into 2D structures such as membranes, *ii*) the functionalities defining the hydrophobicity of the rod (but also the possible interactions with the dyes) can be tailor-made for the particular application, and *iii*) no formation of super-structures, *e.g.*, as in case of polypeptides (*cf.* ternary and quaternary structures) will additionally influence the spatial orientation of dyes attached to the OSK rods [1c][1d][3][4]. Due to its 'pure chemical' character,

additional modifications, *i.e.*, increasing (or decreasing) the solubility of the OSK construct or disabling (enabling) specific (bio)chemical properties of the OSK rod, can be envisaged (*e.g.*, no biodegradation by enzymes; hydrophobic structure that can be used to anchor molecules, which may serve as a recognition elements in membranes) [2c][2d].

In the present interdisciplinary work, the synthesis of the dye-labeled OSK rod constructs (labeled with carboxyfluorescein (FLU), carboxyrhodamine (RHO), pyrene (PYR), and perylene (PER) structures) as well as their fundamental photophysical characterization are reported. Special emphasis is given to OSK rod constructs labeled with the dye pairs FLU/RHO or PYR/PER, respectively. Here, the potential of OSK rods as specifically designed spacers in FRET applications is investigated. The rotation of the fluorescence probe, the properties of the linker attaching the dye to the OSK rod, as well as the rigidity of the OSK rod itself are major parameters determining the performance of the OSK rod constructs as FRET spacers and were characterized in detail. In a first set of experiments, the dye-labeled OSK rods were introduced to CTAB (cetyltrimethylammonium bromide) micelles as simple biomimetic model, and the photophysics was investigated as well.

Results and Discussion. – *Synthesis of the Rod Constructs.* The synthesis of dye-labeled oligospiroketal (DOSK) rods is based on stepwise Cu-catalyzed alkyne–azide cycloaddition (CuAAC, 'click' reaction) of ω,ω'-diazido rods **1** with ethynyl-substituted dyes **2** [5]. To evaluate the influence of the rod length on the photophysical behavior of DOSK rods, two diazido rods, **1a** and **1b**, have been chosen with different lengths. The long rod (LR) **1b** was previously described [2b], for the short rod (SR) **1a**, the reader is referred to the *Exper. Part*. The general approach and the formulae of the reactants **1** and **2** are depicted in *Scheme 1*.

For the preparation of single-labeled rods **3**, the diazido rods **1a** or **1b** were subjected to the CuAAC with 1.1 equiv. of alkynes **2a**/**2b**, whereas the double-labeled rods **4** were obtained by treatment of **1a** or **1b** with 1:1 mixtures **2a**/**2b** or **2c**/**2d**, and separation of the resulting product mixture. In both cases, the previously reported catalyst Cu/C was employed [6]. The formulae of the eight DOSK rods obtained by this procedure are given in *Fig. 1*. Compounds **3e** and **3f** were used as reference for the elucidation of the photophysical processes.

Investigation of Förster *Resonance Energy Transfer* (FRET) *in Double-Labeled DOSK Rods.* In the course of designing novel probes for sensing applications, different dye molecules were attached to OSK rods to obtain double-labeled DOSK rods by the 'click' reaction.

As a first sample, PYR and PER were attached to the opposite ends of the OSK rods (see *Scheme 1*). PYR is a well-known fluorescence probe for monitoring its molecular environment (*e.g.*, in membranes) [7]. Depending on the polarity, the ratio of fluorescence bands as well as its fluorescence decay time are altered. In combination with PER, an intriguing FRET pair is created. In this donor–acceptor pair, the PYR with its outstandingly long fluorescence decay time acts as the energy donor (D) and should stamp its decay kinetics on PER (acceptor (A)), which subsequently should be of great benefit with respect to an advanced two-color time-gated detection scheme. Based on the fundamental photophysical parameters of the PYR and PER compounds,

Scheme 1. *Preparation of Dye-Labeled Oligospiroketal* (DOSK) *Rods* **3** *and* **4**

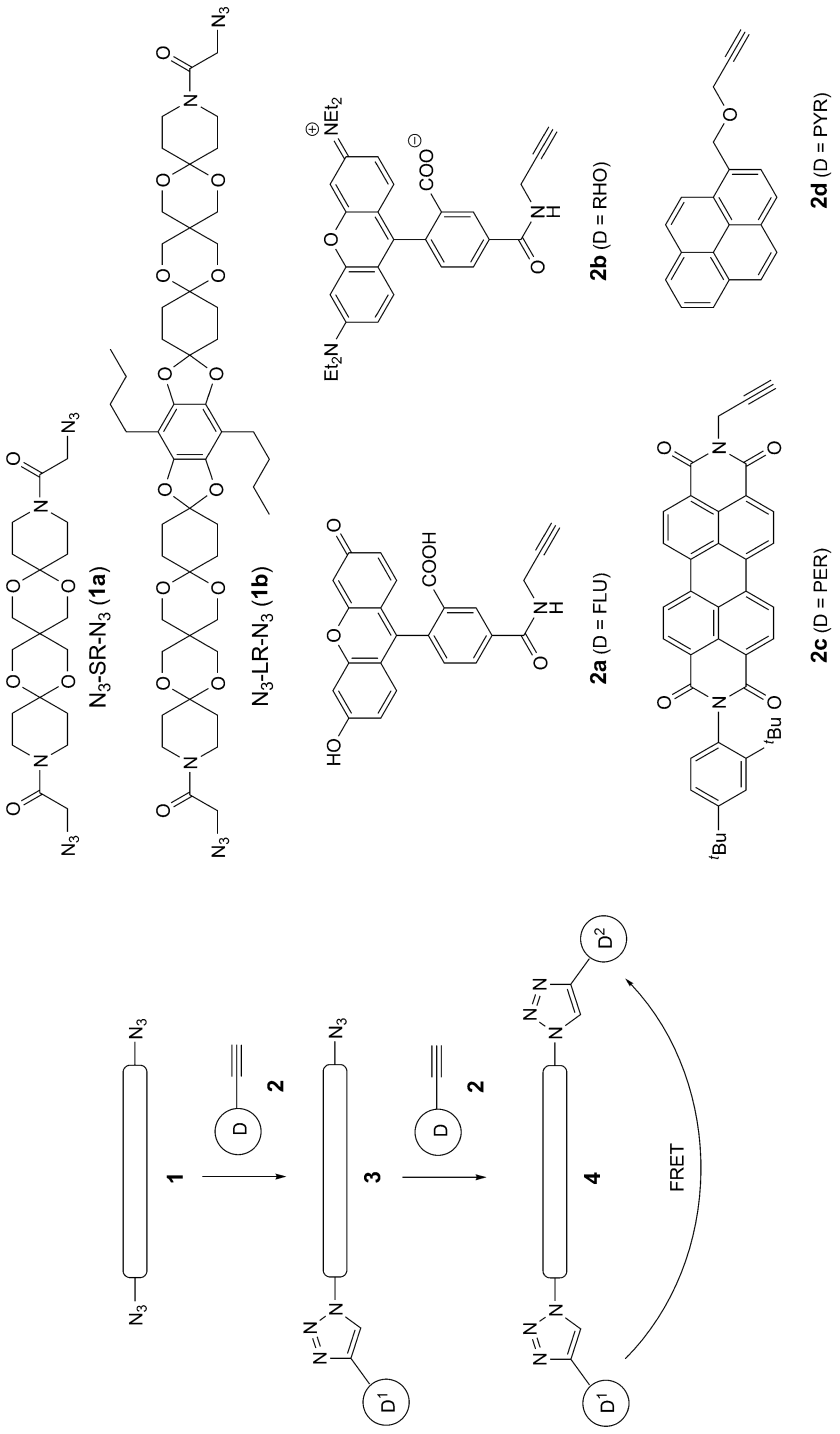

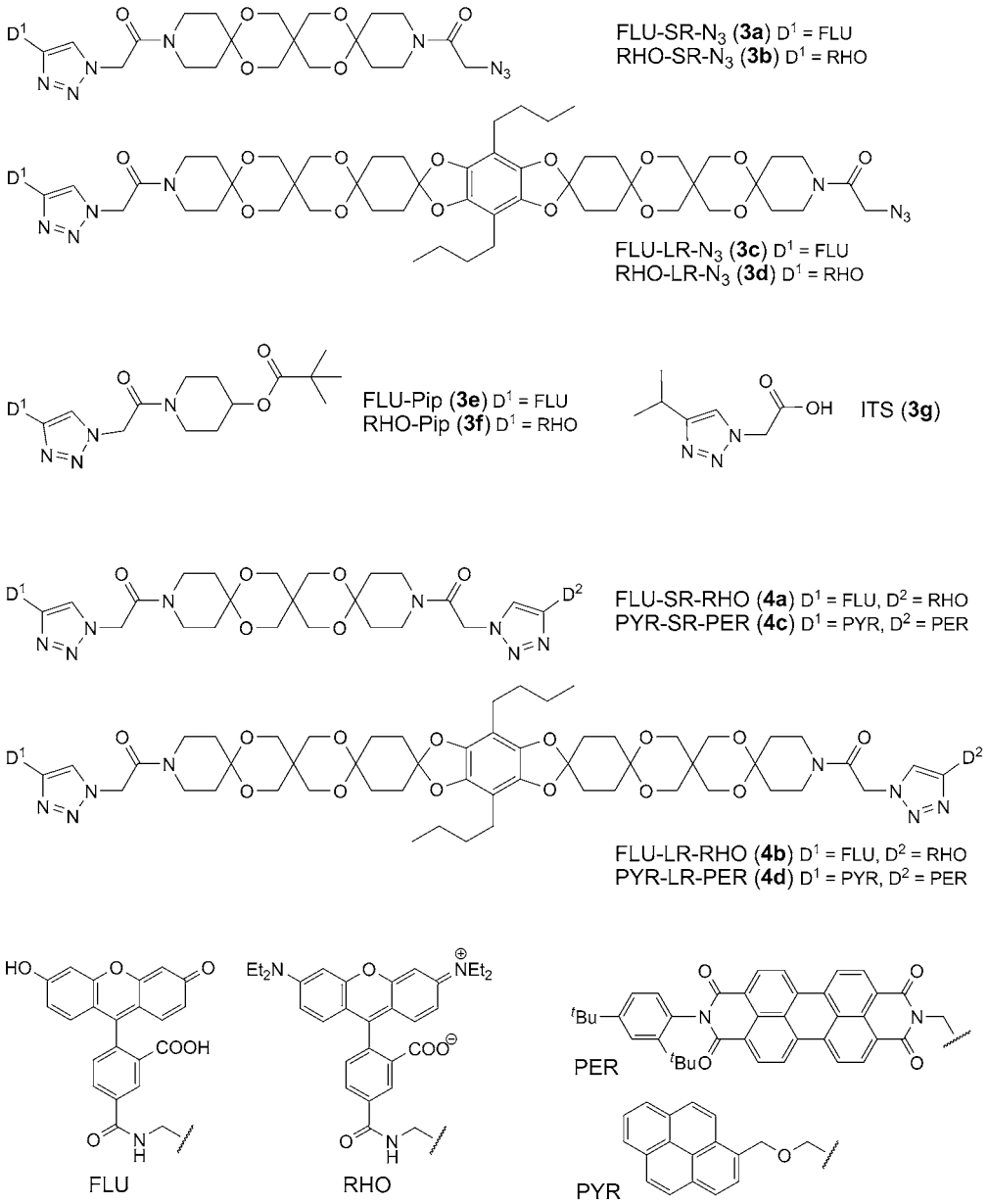

Fig. 1. *Single-labeled DOSK rods* **3a**–**3d**, *investigated reference compounds* **3e**–**3g**, *and double-labeled DOSK rods* **4a**–**4d**

a *Förster* distance, R_0, of 2.2 nm was calculated. In combination with the theoretical length of the OSK rods, energy-transfer efficiencies, E^C, of 0.59 and 0.03 for the short (SR) and long (LR) OSK rod, respectively, were expected (see *Table 1*).

Table 1. *FRET Efficiencies of the Samples Determined from Time-Resolved Fluorescence Spectroscopy* (E^{τ}) *and Calculated for* $R_0 = 2.2$ *nm, and the Distances* R *between Donor and Acceptor* ($R = 2.1$ and $R = 4.0$ nm for **4c** and **4d**, resp.)

Sample	E^{c}	E^{τ}
PYR-SR-PER (**4c**)	0.59	0.36
PYR-LR-PER (**4d**)	0.03	0.2

In the stationary emission measurements, the typical behavior expected for a successful FRET process was observed: *i*) upon excitation of the PYR (D), an enhanced PER (A) emission was detected, *ii*) in the fluorescence excitation spectrum with the detection wavelength set to a PER emission wavelength, the spectral features of PYR were measured, and *iii*) the fluorescence-decay time of PYR was quenched. But the most convincing observation was the increased fluorescence decay time of PER in the double-labeled DOSK rods. In *Fig. 2*, the fluorescence-decay curves of **2c**, and the double-labeled DOSK rods **4c** and **4d** are shown.

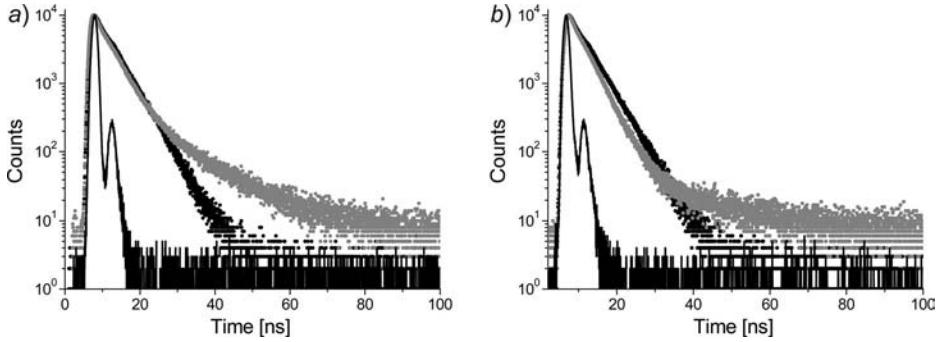

Fig. 2. a) *Fluorescence-decay curves of PER derivative* **2c** (black, λ_{exc} 447 nm) *and PYR-SR-PER* (**4c**; grey, λ_{exc} 254 nm) *in* CH_2Cl_2. b) *Fluorescence-decay curves of* **2c** (black, λ_{exc} 447 nm) *and PYR-LR-PER* (**4d**; grey, λ_{exc} 254 nm) *in* CH_2Cl_2. The emission was detected at λ_{em} 536 nm. The IRF is indicated as black line.

Measuring the fluorescence decay of PER under indirect excitation conditions (after energy transfer from PYR), a considerable increase in the fluorescence-decay time of the PER was observed, which directly points toward a successful FRET process (see *Fig. 2*). The effect was strongest for the short OSK rod. Based on the time-resolved fluorescence measurements, the experimentally apparent FRET efficiencies, E^{τ}, were calculated. In *Table 1*, the calculated and experimental FRET efficiencies are compared. Calculated and experimental values do not match at all. The values of E^{C} were calculated on the assumption that the DOSK rods are present in an extended linear configuration. However, because of solubility constraints the dye molecules could fold back and interact with the OSK rod. In simple molecular-dynamics (MD) simulations[1]), a possible contribution of such folding was found for **4c** and **4d**. The

[1]) MD Simulations were performed with the MMFF94x using the program MOE 2010.

observed differences can be a result of such unexpected conformations, *e.g.*, in case of **4d**, a folded conformation would lead to much smaller distances between the pyrene and perylene moiety, and subsequently, compared to the theoretically expected, a higher energy-transfer efficiency would be observed. On the other hand, due to intramolecular interactions, a limitation with respect to the dye–dye orientation could result in an altered κ^2 value, which in turn could be responsible for the low efficiency observed for **4c**.

Since the aim is to use the DOSK rods in life-science applications, the solubility of the constructs in aqueous solutions was a major concern. Moreover, for the application in microscopy-based methods the use of well-established xanthene dyes such as FLU and RHO is beneficial. Both dyes have been used as FRET pair successfully before [8]. Therefore, in the course of developing novel constructs as FRET probes for life-science applications, double-labeled DOSK rods containing FLU and RHO at the opposite ends of the rod were constructed. As in the case of the PYR/PER FRET construct, the DOSK rods FLU-SR-RHO (**4a**) and FLU-LR-RHO (**4b**) were characterized in steady-state and time-resolved fluorescence measurements, and in addition by single-molecule spectroscopy with respect to their FRET performance. Based on the results obtained for **4c** and **4d**, the measurements were carried out in different solvents: *i*) MeOH, *ii*) MeOH/NaOH, and *iii*) in CTAB micelles as a first simple biomimetic model system for membranes.

In *Fig. 3*,*a*, the absorption spectra of single (*i.e.*, **3a** and **3c**) and double-labeled DOSK rods (*i.e.*, **4a**) are compared.

From *Table 2*, it can be seen that the absorption and emission maxima of the double-labeled DOSK rods **4a** and **4b**, compared to the corresponding single-labeled DOSK rods, are not altered. The absorption spectrum of the double-labeled DOSK compound **4a** (and **4b**) comprises of the absorption spectra of FLU and of RHO, respectively (see *Fig. 3*,*a*).

Based on the spectroscopic properties of the FLU- and RHO-labeled DOSK rods (quantum efficiency of FLU, extinction coefficient of RHO, spectral overlap integral,

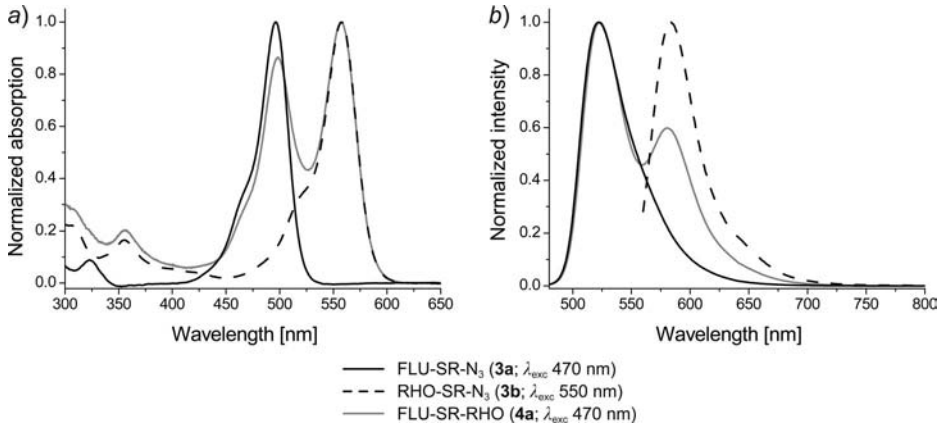

Fig. 3. a) *Normalized absorption spectra and* b) *steady-state fluorescence emission spectra of labeled DOSK rods in 1 mM NaOH/MeOH.*

Table 2. *Fundamental Photophysical Parameters in Different Solvents.* λ_{abs}, Absorption maximum; λ_{em}, emission maximum; Φ_F, fluorescence quantum efficiency; τ, fluorescence decay time.

Sample	MeOH				NaOH/MeOH				CTAB			
	λ_{abs} [nm]	λ_{em} [nm]	Φ_F [%]	τ [ns][a])	λ_{abs} [nm]	λ_{em} [nm]	Φ_F [%]	τ [ns][a])	λ_{abs} [nm]	λ_{em} [nm]	Φ_F [%]	τ [ns][a])
FLU	485	520	59	4.1[b])	494	519	86	4.2[b])	503	529	80	4.8[b])
FLU-SR-N_3 (**3a**)	481	520	44	4.1[b])	496	522	77	4.1[b])	506	530	79	4.5[b])
FLU-LR-N_3 (**3c**)	488	525	39	4.0[b])	497	524	76	4.3[b])	506	537	73	4.6[b])
FLU-Pip (**3e**)	485	522	59	4.3[b])	497	522	84	4.3[b])	506	532	83	4.6[b])
RHO	545	569	45	2.1[c])	553	576	40	1.8[c])	554	577	39	2.2[c])
RHO-SR-N_3 (**3b**)	550	582	44	1.7[c])	557	587	38	2.5[c])	559	576	38	2.6[c])
RHO-LR-N_3 (**3d**)	547	562	46	2.3[c])	554	574	–	2.1[c])	553	568	46	2.6[c])
RHO-Pip (**3f**)	548	574	45	2.5[c])	557	583	35	2.2[c])	557	582	41	2.6[c])
FLU-SR-RHO (**4a**)	485	518		4.0[b])	498	523		4.1[b])	509	530		4.2[b])
	550	574	42	1.8[c])	557	581	38	2.4[c])	557	582	34	2.6[c])
FLU-LR-RHO (**4b**)	485	521		4.1[b])	502	521		4.0[b])	512	531		4.3[b])
	548	569	45	2.4[c])	555	570	–	2.2[c])	553	567	37	2.6[c])

[a]) The error in the decay time determination is ± 0.1 ns. [b]) λ_{exc} 470, λ_{em} 505 nm. [c]) λ_{exc} 55 and λ_{em} 620 nm.

Table 3. *Calculated* Förster *Distance* (R_0) *and Overlap Integral* (J) *Values for the Samples in Different Solvents* ($\Phi_{F,D}$, fluorescence quantum yield of the donor determined with single-labeled constructs). The *Förster* distance, R_0, was calculated with the orientation factor $\kappa^2 = 2/3$. FRET Efficiencies [%] of the samples in different solvents determined with steady-state (E^E), time-resolved (E^τ), single molecule (E^S) fluorescence spectroscopy, and calculated with the values for R_0 and the distances between donor and acceptor ($R = 1.9$ and $R = 3.8$ nm for **4a** and **4b**, resp.).

	FLU-SR-RHO (**4a**)			FLU-LR-RHO (**4b**)		
	MeOH	NaOH/MeOH	CTAB	MeOH	NaOH/MeOH	CTAB
n	1.33345	1.34348	1.34014	1.33345	1.34348	1.34014
$\Phi_{F,D}$ [%]	44	77	79	39	76	73
J [10^{15} M^{-1} cm^3]	3.63	4.06	5.6	4.36	4.38	6.21
R_0 [nm]	5.8	6.2	6.6 (6.2)[a]	5.6	6.3	6.6 (6.2)[a]
E^E	22	26	24	13	13	14
E^τ	n.m.[b]	n.m.[b]	8	5	6	8
E^S	n.d.[c]	30	85 ± 10	n.d.[c]	10	67 ± 7
E^C	100	100	100 (100)[a]	91	95	97 (95)[a]

[a]) R_0 in CTAB was calculated with $\kappa^2 = 0.475$ according to [11]. [b]) n.m., No difference between single- and double-labeled constructs in the observed FLU decay time. [c]) n.d., Not determined for MeOH due to experimental constrains.

and based on the anisotropy data set $\kappa^2 = 2/3$, *vide infra*), the critical *Förster* distance, R_0, was calculated (see *Table 3*). The calculated values of R_0 for **4a** and **4b** were found to be well within the range of reported values for derivatives of this donor–acceptor pair (carboxyfluorescein–tetramethylrhodamine: $R_0 = 5.1$ nm [7a]; carboxyfluorescein–sulforhodamine B: $R_0 = 5.8$ nm [9]; 5-(*N*-hexadecanoylamino)fluorescein–octadecylrhodamine B: $R_0 = 5.4$ nm [10]). Depending on the solvent used, a critical *Förster* distance of 5.6 nm $< R_0 <$ 6.6 nm was calculated for the double-labeled DOSK rods. Under the assumption of a rigid OSK rod (with the dye linkers in a stretched conformation), the distance between FLU and RHO moiety was calculated, and a theoretical FRET efficiency E^C was determined. From *Table 3*, it can be seen that, for FLU-SR-RHO (**4a**), almost 100% transfer efficiency is expected, while for the FLU-LR-RHO (**4b**) *ca.* 80% are predicted.

A first experimental indication for successful FRET between FLU and RHO in **4a** and **4b** was obtained from the fluorescence excitation spectra. Here, with the detection wavelength set on an acceptor emission wavelength, the excitation spectrum was found to be a combination of the spectral features of RHO and FLU (see *Fig. 4,a*). Also, for **4a** and **4b** a distinct reduction of the FLU-related fluorescence intensity and a simultaneous enhancement of the RHO-related emission were observed when compared to the single-labeled DOSK rods (see *Fig. 4*, *left* and *right*, for the different OSK rods of SR and LR length, resp.). However, independent on the solvent, FRET efficiencies of only *ca.* 24 and 13% were calculated for **4a** and **4b**, respectively, from the evaluation of the steady-state fluorescence measurements. Moreover, no quenching of the FLU fluorescence-decay time was found for FLU-SR-RHO (**4a**), and for FLU-LR-RHO (**4b**) only a slight decrease in the fluorescence-decay time of FLU was found. In that case, based on the decrease in the fluorescence-decay time, a FRET efficiency, E^τ,

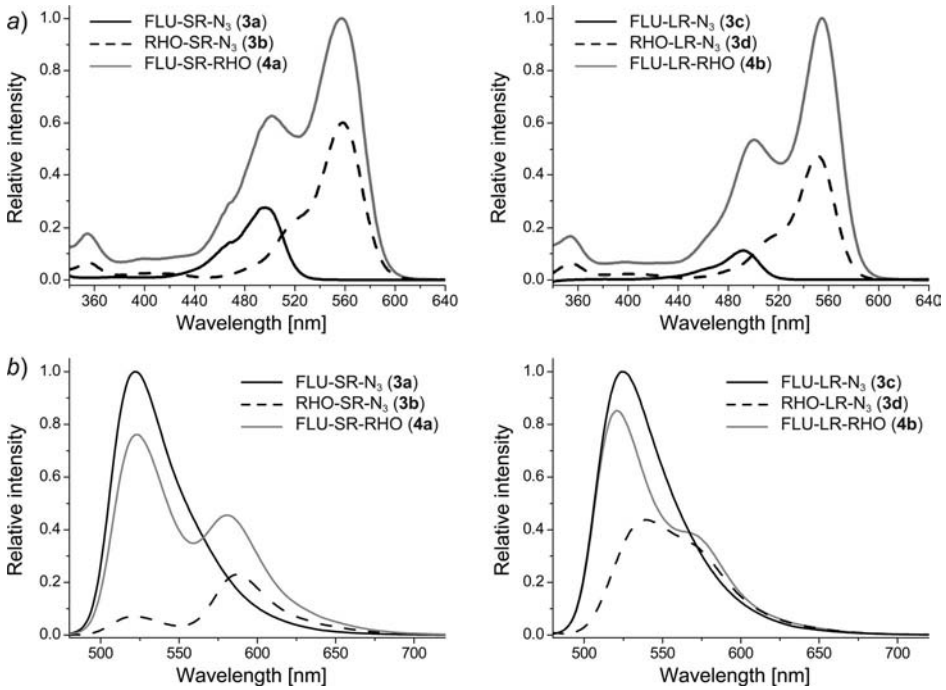

Fig. 4. a) *Steady-state fluorescence excitation spectra* (λ_{em} 650 nm) *and* b) *fluorescence emission spectra* (λ_{exc} 470 nm) *of the single- and double-labeled DOSK Rods in 1 mM NaOH/MeOH*

of only *ca.* 5% was determined. Likewise, for the PYR/PER-labeled DOSK rods the experimentally determined energy-transfer efficiencies (E^{τ}, E^{E}) were considerably different from the theoretically predicted (E^{C}; see *Table 3*). In addition to the ensemble fluorescence measurements, single-molecule fluorescence experiments were performed in NaOH/MeOH, and the data fit well with the ensemble measurements (see *Table 3* and *Fig. 5*).

The results strongly point towards a strong contribution of a static-like (proximity) quenching between FLU and RHO in the doubled-labeled rods, as observed before [11]. In the double-labeled DOSK rods, even though FLU and RHO show a decent water solubility a folding of the dye molecules towards the OSK rod moiety has been found in MD simulations. From this folding process, two subpopulations (unfolded *vs.* folded) may arise (*Fig. 6*).

The proximity quenching would be observed preferentially for the folded subpopulation and should be especially effective in FLU-SR-RHO (**4a**) and slightly less operative in FLU-LR-RHO (**4b**), due to the increased distance between the two dyes. From the finding that the reduction in the FLU fluorescence intensity is accompanied by an increase in the RHO fluorescence intensity, it may be concluded that the underlying mechanism of the observed fluorescence quenching is still an energy-transfer process. Using the calculated R_0 value and *Eqn. 1* to obtain an estimate for the rate constant of the energy transfer step, a $k_{ET} > 10^{10}$ s^{-1} is found for **4a**. This is

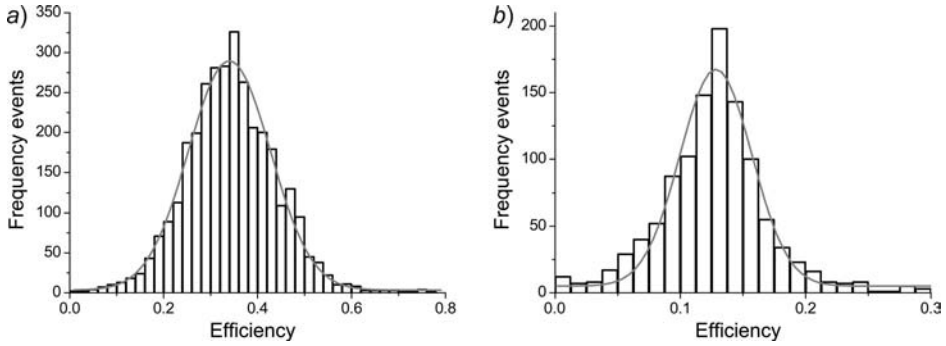

Fig. 5. *FRET Histogram extracted from single-molecule experiments for* a) *FLU-SR-RHO* (**4a**) *and* b) *FLU-LR-RHO* (**4b**) *in 1 mM NaOH/MeOH* (λ_{exc} 470 nm). The data were fitted according to a *Gaussian* distribution (grey line).

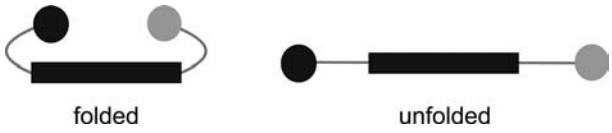

Fig. 6. *Two examples of possible subpopulations* (folded and unfolded). The OSK rod is shown as a black rectangle, and the dyes are symbolized by grey and black circles.

about an order of magnitude faster than the rate constant of the corresponding fluorescence process.

$$k_{ET} = \frac{1}{\tau_D^0} \cdot \left(\frac{R_0}{R}\right)^6 \quad (1)$$

In such a case, large differences between steady-state and time-resolved data can be found. The time-resolved measurements 'see' only a less-quenched fraction (which is present, *e.g.*, due to conformational changes a negative influence of κ^2 could reduce the effective rate constant k_{ET} for that fraction of molecules). A second possibility is that an additional quenching mechanism such as photoinduced electron transfer becomes operative, when the two fluorophores are in closer proximity. Here, the presence of the triazole moiety of the DOSK needs to be taken into account. A rough estimation based on the redox properties of FLU (oxidation potential $E_{Ox} = -1.19$ V) and RHO (reduction potential $E_{Red} = -0.95$ V) showed that it could be feasible (yielding a free enthalpy ΔG *ca.* -2.7 V according to *Rehm–Weller*) [3d][12][13].

To further explore the distinct differences between calculated and experimentally obtained energy-transfer efficiencies for the double-labeled DOSK rods, a set of reference compounds, **3e** and **3f**, was investigated (*Fig. 1*). Especially, the influence of additional intramolecular interactions (*e.g.*, triazole ring) on the fluorescence properties was investigated in more detail.

Photophysical Characterization of the Single-Labeled DOSK Rod Constructs. In the *Huisgen* [3+2] cycloaddition reaction, a 1,2,3-triazole ring is formed, which could

introduce 'extra' (photophysical) properties interfering with the wanted FRET process in the double-labeled DOSK rods. The N-atoms can actively participate in complexation reactions (*e.g.*, with solvent molecules, *etc.*) *via* their lone electron pairs, *e.g.*, acting as electron donor or as partners in H-bonding. Moreover, the C–H group has a decent acidic character, which further makes the 1,2,3-triazole ring a possible partner in intra- and intermolecular interactions [14].

The absorption and emission spectra of the parent fluorescence dyes as well as of the DOSK rods **3a**–**3d** (see *Fig. 1*) were recorded in MeOH, NaOH/MeOH (see *Fig. 3*), and in CTAB/PBS (phosphate buffered saline). The fundamental photophysical parameters of the samples are compiled in *Table 2*.

Upon coupling to the OSK rods (SR or LR), only weak-to-moderate alterations in the fundamental photophysical parameters of the dyes were observed compared to the respective parent compounds (see *Table 2*). In going from MeOH to NaOH/MeOH, slight changes in the absorption and emission properties of all DOSK samples, *i.e.*, **3a**–**3d**, were induced. In general, a bathochromic shift of the related absorption and emission maxima as well as a slight increase of the fluorescence decay times were observed. In MeOH and MeOH/NaOH, the FLU-labeled DOSK rods, **3a** and **3c**, showed a decay time of $\tau = (4.1 \pm 0.1)$ ns, and for the RHO labeled DOSK rods, **3b** and **3d**, a decay time $\tau = (2.0 \pm 0.3)$ ns was determined, which were slightly increased compared to those of the parent compounds, FLU and RHO, under similar solvent conditions. The fluorescence quantum yields of the dyes in the single-labeled DOSK rods were slightly decreased in the case of FLU and not changed for RHO. A distinct alteration of the spectra was found for the RHO-labeled DOSK rods. In the fluorescence spectrum of the RHO-SR-N_3 (**3b**) and RHO-LR-N_3 (**3d**), a weak new fluorescence band at shorter emission wavelengths (λ_{exc} 470, λ_{em} 520 nm) was observed. To further evaluate this alteration in the fluorescence spectrum of the samples **3b** and **3d**, the influence of unbound 2-(4-isopropyl-1*H*-1,2,3-triazol-1-yl)acetic acid (ITS; **3g**; as model for the 1,2,3-triazole ring) on the photophysical properties of the parent compounds, FLU and RHO, was investigated. It was found that the fluorescence-decay time of FLU slightly decreased with increasing **3g** concentration, and that in the fluorescence spectra of RHO an additional emission signal arose upon addition of **3g** ($\lambda_{em} \approx 520$ nm). This is comparable to the changes observed for the RHO-labeled DOSK rods, **3b** and **3d**. From these observations, it can already be concluded that the observed slight modifications observed for the photophysical properties of the FLU- (*i.e.*, **3a** and **3c**) and RHO-labeled DOSK rods (*i.e.*, **3b** and **3d**) are connected to the presence of the 1,2,3-triazole ring in the DOSK rods.

To further investigate possible intramolecular interactions, such as stacking of the dyes on the OSK rod, time-resolved fluorescence depolarization measurements were performed. For MeOH and NaOH/MeOH solutions, the anisotropy decays of the different samples were analyzed using a single exponential decay law (see *Eqn. 3*). The results are collected in *Table 4*. It can be seen that the obtained rotational correlation times φ for FLU and RHO are only slightly increased upon linkage to the OSK rod. No significant change in the anisotropy-decay kinetics was observed, probably due to the fact that the differences in size of the rotational volume between the parent molecules (FLU and RHO) and DOSK rods **3a**–**3d** were too small to cause a significant change in the rotational correlation time φ. Consequently, no further conclusions, *e.g.*,

Table 4. *Rotational Correlation Times φ of the Samples in Different Solvents.* For the CTAB solution, the two-step and wobbling-in-cone model parameters (structure parameter *S*, wobbling angle θ) obtained from the analysis of time-resolved anisotropy experiments are shown. Fluorescence-anisotropy measurements for FLU and FLU-labeled DOSK rods were performed at λ_{exc} 470 and λ_{em} 529 nm, while for RHO and RHO-labeled DOSK rods λ_{exc} 550 and λ_{em} 620 nm were used, respectively. For the calculation of φ_L *Eqn. 5* was applied using a rotational correlation time of the micelle, φ_M of 21 ns [15], which was calculated based on the hydrodynamic radius determined in fluorescence correlation spectroscopy experiments.

Sample	MeOH	NaOH/MeOH	CTAB					
	φ [ns]	φ [ns]	φ_{fast} [ns]	φ_{slow} [ns]	φ_L [ns]	φ_w [ns]	*S*	θ [°]
FLU	0.3	0.3	0.7	3.9	4.8	0.8	0.6	46
FLU-SR-N_3 (**3a**)	0.4	0.6	1.1	5.3	7.1	1.4	0.7	38
FLU-LR-N_3 (**3c**)	0.3	0.5	1.2	4.6	5.9	1.5	0.7	38
RHO	0.3	0.4	1.1	8.5	14.4	1.2	0.6	49
RHO-SR-N_3 (**3b**)	0.4	0.6	0.7	7.3	11.2	0.8	0.8	31
RHO-LR-N_3 (**3d**)	0.4	0.7	0.7	7.5	11.7	0.7	0.8	31
FLU-SR-RHO (**4a**)[a])	0.5	0.6	0.9	6.4	9.2	1.0	0.8	31
	0.5	0.7	0.6	6.7	9.9	0.7	0.9	26
FLU-LR-RHO (**4b**)[a])	0.4	0.7	0.9	5.7	7.8	1.1	0.7	38
	0.4	0.6	0.8	7.7	12.2	1.0	0.8	33

[a]) First line: λ_{exc} 470, λ_{em} 529 nm; second line: λ_{exc} 550, λ_{em} 620 nm.

regarding possible stacking between dye molecule and OSK rod, can be drawn from these data.

DOSK Rods as Membrane Probes. The DOSK rods were investigated in the presence of CTAB micelles, which served as a first simple robust model for membranes. In the CTAB solution, all DOSK rods were readily incorporated into the micelles. The addition of the cationic detergent CTAB induced a slight alteration in the spectroscopic properties of the FLU-labeled DOSK rods **3a** and **3c**. A bathochromic shift in the absorption and fluorescence spectrum was found for the FLU fluorophore, and can be attributed to the specific interaction of the FLU fluorophore with the CTAB micelles (inclusion of the FLU probes into the micelle). Comparable spectral shifts were reported before for the parent compound FLU and other FLU probes such as 5-(hexadecanoylamino)fluorescein (HAF) in micellar CTAB solutions [15]. In addition, also an increase in the fluorescence-decay times of the single-labeled DOSK rods **3a** – **3d** was found upon incorporation in CTAB micelles (see *Table 2*).

To further investigate the incorporation of DOSK rods in micelles, time-resolved fluorescence anisotropy measurements were carried out. In *Fig. 7*, the fluorescence anisotropy decay of the double-labeled DOSK rods is shown. The anisotropy decay was measured for the FLU and RHO part of the double-labeled DOSK rods under selective excitation and emission conditions, respectively. The comparison reveals only slight differences between the rotational correlation times φ of the single-labeled DOSK rods and the dyes in the respective double-labeled DOSK rods (see *Table 4*).

In CTAB micelles, the fluorescence anisotropy decay of the parent compounds as well as of the DOSK rods became connected to the overall motion of the micelle. The

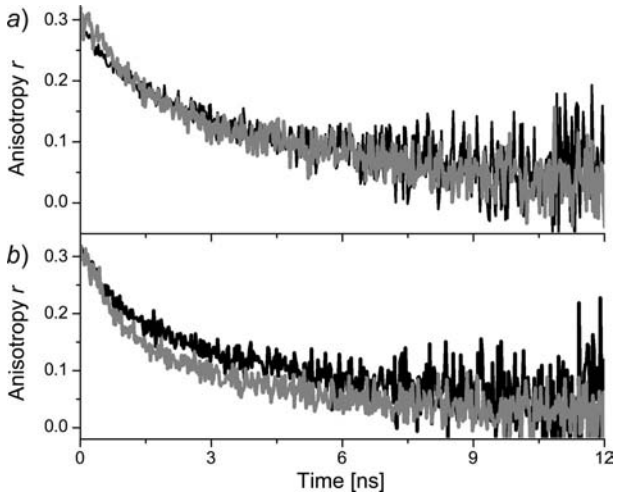

Fig. 7. *Anisotropy decay of the double-labeled DOSK rods.* The anisotropy was measured for FLU as well as for RHO. Shown are the anisotropy decays of both dyes under selective excitation (grey: λ_{exc} 470, λ_{em} 529 nm; black: λ_{exc} 550, λ_{em} 620 nm) in 1 mM CTAB/PBS solution at 294 K. *a*) FLU-SR-RHO (**4a**); *b*) FLU-LR-RHO (**4b**).

finding, that complex anisotropy decay kinetics is observed, already indicates that the DOSK rods are not rigidly attached/incorporated to/in the micelles. Applying the wobble-in-cone model (see *Eqns. 4–6* in the *Exper. Part*), the rotational and translational diffusion of the DOSK rod in a micellar environment was analyzed [16]. For the determination of the contributions of the different rotational and translational motions as well as of the order parameters (S, θ), and to reduce the number of free parameters in the evaluation of the anisotropy data, the overall rotational correlation time of the micelle, φ_M, was determined based on fluorescence correlation spectroscopy experiments (using the size of the CTAB micelles to calculate φ_M). The analysis of the anisotropy decay of the parent compounds yielded rotational correlation times and order parameters, which were in good agreement with literature values of the same or similar compounds (see *Table 4*) [16]. For the FLU-labeled DOSK rods, an increase of the fast and slow rotational motion was found, while for the RHO-labeled DOSK rods a slight decrease was observed. The differences in the corresponding rotational correlation times between the short (SR) and long (LR) DOSK rods were small. The calculated order parameters (and the corresponding wobble-in-cone angle) indicate that the rotational freedom of the dyes decreased upon labeling to the OSK rod. The fluorophores may still reside in the interfacial layer between micelle and bulk solution, but the rod can act like an anchor reducing the overall rotational freedom of the labeled dyes. Moreover, for the double-labeled DOSK rods **4a** and **4b**, the observed energy-transfer efficiency, E^S, increased, especially, when measured in single-molecule fluorescence experiments. Here, E^S nearly approached the calculated value E^C. Steady-state fluorescence as well as single-molecule fluorescence measurements (SMS) are intensity-related methods, but the latter technique has the advantage that the averaging-out due to observation of a

fluorophore ensemble can be avoided. Thus, SMS enables the resolution and detection of subpopulations. In CTAB micellar solutions, the equilibrium between the subpopulations seems to be shifted towards the unfolded configuration due to an improved solubility of the doubled-labeled DOSK rods in the micelles. Subsequently, the proximity quenching is relaxed and the 'expected' energy transfer between the donor–acceptor pair is now observed.

Conclusions. – The combination of OSK rods and fluorescence probes enables design of novel tailor-made FRET probes with scalable distances between donor and acceptor without the necessity of using bulky biomolecules (*e.g.*, proteins or DNA). Especially, the relatively low molecular weight of the rod is very attractive for the construction of standards for FRET investigation or for novel probe systems applicable in competitive fluorescence assays. Compared to bimolecular spacers, the dimensions of the OSK rods are smaller, and moreover, the 'chemical surface' of the rod can be adapted (*e.g.*, with respect to polarity), which can be a further benefit for the design of novel probes for life sciences. The DOSK rods can be envisaged for the investigation of membranes and transmembrane processes. Attaching different reporters to the opposite ends of the OSK rods, transmembrane processes involving a first messenger situated outside the cell and stimulating a second messenger inside the cell can be studied. As a first confirmation of the principle, the induced FRET of the double-labeled DOSK rods in micelles was discussed (here, the first messenger is a photon absorbed by the donor, and the second messenger is also a photon (of different color), which is emitted by the acceptor.

The specific influences of structural elements arising for dye-labeling chemistry need to be controlled very carefully. FLU and RHO are frequently used fluorescence probes in life-science applications. However, due to their chemical nature, intra- and intermolecular interactions with parts of the OSK rod are possible. For the OSK rods designed in the present study, depending on the properties of the dyes attached to the rod moiety, specific interactions with 1,2,3-triazole ring or the OSK rod itself were shown to be of major influence. For the FLU-RHO dye pair, the combination of ensemble and single-molecule fluorescence experiments revealed that, in the double-labeled DOSK rods, a combination of proximity and dynamic quenching is present, which underlines the necessity *i*) to perform case-to-case studies for the probes used in combination with the specific OSK rod architecture and *ii*) to apply complementary experimental techniques in the characterization of the FRET probes.

The financial support of this work by the *Deutsche Forschungsgemeinschaft* (We1850-7/1-2) is gratefully acknowledged. *M. U. K.* is grateful to *J. von der Bever* for discussions on lifetime evaluations.

Experimental Part

General. (Hexadecyl)(trimethyl)ammonium bromide (CTAB; *CAS:* 57-09-0; $\geq$99.0%) and 5(6)-carboxyrhodamine (RHO; *CAS:* 81-88-9; $\geq$97.0%) were purchased from *Sigma-Aldrich* (DE-Deisenhofen), 5(6)-carboxyfluorescein (FLU; *CAS:* 72088-94-9) was obtained from *Invitrogen* (DE-Karlsruhe). Stock solns. of the samples were prepared in MeOH, in a soln. of 1 mM NaOH/MeOH, 3:1, and in 1 mM CTAB/PBS (physiological buffered saline, pH 7.4). Samples investigated were *i*) free dyes (FLU and RHO), *ii*) molecular rods containing either FLU or RHO (FLU-SR-N_3 (**3a**), RHO-SR-N_3

(**3b**), FLU-LR-N_3 (**3c**), RHO-LR-N_3 (**3d**)), *iii*) molecular rods containing FLU as well as RHO (FLU-SR-RHO (**4a**) and FLU-LR-RHO (**4b**)), and *iv*) molecular rods containing PYR as well as PER (PYR-SR-PER (**4c**) and PYR-LR-PER (**4d**)). The refractive indices of MeOH, NaOH/MeOH, and CTAB solns. were determined using a digital multiple-wavelength refractometer (*DSR-λ*, *Schmidt and Haensch*, DE-Berlin) at λ of 470 nm (293 K). The error of the measurements was determined from repeated measurements as ± 0.0004.

OSK-Rod Construct Synthesis. All reactions using dry solvents were performed under N_2 in heat gun-dried flasks. The solvents were dried and distilled prior to use by usual laboratory methods. All reagents obtained from commercial sources were used without further purification. TLC: silica-gel plates (*Merck*, silica gel *60* F_{254}). Flash chromatography (FC): silica gel (*Merck Geduran Si 60*, 40–63 μm). Prep. NP-HPLC: *Eurospher 100* column (*Knauer*, 5 μm, 32 × 250 mm) in a isocratic mode over 20 min at a flow rate of 32 ml/min with UV detection at 254; used for the products **4c** and **4d**. The crude products **3a**–**3c** and **4a** were purified by semi-prep. RP-HPLC on an *Eurosil*, *Bioselct-300* C_{18} column (*Knauer*, 10 μm, 16 × 250 mm) with a linear gradient program from 20–90% *B* over 30 min (solvent *A:* H_2O 0.05% CF_3COOH; solvent *B:* MeCN 0.05% CF_3COOH) at a flow rate of 16 ml/min. The purification of product **4b** was carried out on a *Sephadex LH 20* (*GE Healthcare*, UK-Buckinghamshire) column (15 × 60 mm) in CH_2Cl_2/MeOH 1:1. For the purification of products **3e** and **3f**, the same method was used with *Sephadex LH 20* and MeOH. M.p.: *Elektrothermal 9100*; uncorrected. IR Spectra: as KBr pellets or as films; *Perkin Elmer IR-881* spectrometer. ^{1}H- and ^{13}C-NMR spectra: *Bruker AVANCE 300* and *Bruker AVANCE 500* spectrometer; chemical shifts δ in ppm with TMS as internal standard, coupling constants (*J*) in Hz. ESI-MS: *Bruker maXis QTOF* instrument. MALDI-TOF-MS: *AXIMA*™ *Assurance* (*Shimadzu Biotech*, *Kratos Analytical Limited*, Manchester, UK) time-of-flight mass spectrometer, fitted with 337-nm pulsed nitrogen laser; all spectra were obtained in a positive-ion linear mode, data were processed using the Launchpad 2.8. software package (*Shimadzu Biotech*, *Kratos Analytical Limited*, Manchester, UK); a sat. soln. of sinapinic acid (*Fluka*) in MeCN/H_2O 50:50 + 0.1% CF_3COOH was used as matrix for all samples.

1,1′-(7,11,18,21-Tetraoxa-3,15-diazatrispiro[5.2.2.5^{12}.2^9.2^6]henicosane-3,15-diyl)bis(2-chloroethanone) (**7**). Compound **5** (498 mg, 2.84 mmol, 1.95 equiv.) [2b] and **6** (617 mg, 1.45 mmol) were added to dry Et_2O (25 ml). Trimethylsilyl triflate (= trimethylsilyl trifluoromethanesulfonate (TMSOTf); three drops, 20 μl, 70 μmol, 0.05 equiv.) was added, and the mixture was stirred at r.t. overnight (*Scheme 2*). Monitoring with TLC showed still small amounts of reactants. Dry CH_2Cl_2 (4 ml) and TMSOTf (three drops, 20 μl, 70 μmol, 0.05 equiv.) were added, and the mixture was stirred until TLC showed complete conversion. Brine was added, and the aq. layer was extracted three times with CH_2Cl_2. The combined org. layers were dried ($MgSO_4$), filtered, and evaporated. The resulting residue was purified by FC (CH_2Cl_2/MeOH 100:3) to yield **7** (556 mg, 1.23 mmol, 87%). White foam. R_f (CH_2Cl_2/MeOH 10:1) 0.54. M.p. 172–173°. IR: 3452, 2969, 2939, 2867, 1655, 1444, 1362, 1339, 1269, 1240, 1220, 1166, 1150, 1088, 1059, 1037, 937, 886, 787, 729, 659. ^{1}H-NMR (300 MHz, $CDCl_3$): 1.82–1.91 (*m*, 4 CH_2); 3.46–3.51 (*m*, 2 CH_2); 3.58–3.63 (*m*, 2 CH_2); 3.71 (*s*, 2 CH_2); 3.78 (*s*, 2 CH_2); 4.06 (*s*, 2 CH_2). ^{13}C-NMR (75 MHz, $CDCl_3$): 31.0 (CH_2); 33.0 (C); 33.2 (CH_2); 38.9 (CH_2); 40.9 (CH_2); 42.9 (CH_2); 63.2 (CH_2); 63.3 (CH_2); 96.6 (C); 164.8 (C). HR-ESI-MS: 451.1396 ($[M+H]^+$, $C_{19}H_{29}{}^{35}Cl_2N_2O_6^+$; calc. 451.1397).

Scheme 2. *Synthesis of Compound* **7**

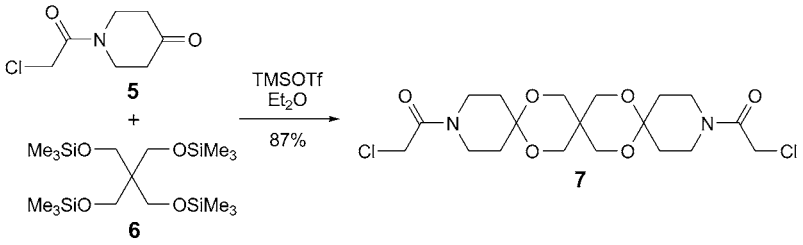

1,1′-(7,11,18,21-Tetraoxa-3,15-diazatrispiro[5.2.2.5^{12}.2^{9}.2^{6}]henicosane-3,15-diyl)bis(2-azidoethanone) (**1a**). Compound **7** (496 mg, 1.10 mmol) was dissolved in dry DMF (6 ml). NaN_3 (159 mg, 2.42 mmol, 2.2 equiv.) was added, and the mixture was stirred 2 h at r.t. Brine was added, and the aq. soln. was extracted three times with CH_2Cl_2. The combined org. layers were dried ($MgSO_4$), filtered, and evaporated. The resulting residue was purified by FC (CH_2Cl_2/MeOH 100:4) to yield **1a** (496 mg, 1.07 mmol, 97%). White solid. R_f (CH_2Cl_2/MeOH 10:1) 0.57. M.p. 171–173°. IR: 3449, 2108, 1642, 1442, 1367, 1268, 1232, 1167, 1151, 1084, 1059, 795. ^{1}H-NMR (300 MHz, $CDCl_3$): 1.80–1.87 (*m*, 4 CH_2); 3.32–3.36 (*m*, 2 CH_2); 3.58–3.63 (*m*, 2 CH_2); 3.69 (*s*, 2 CH_2); 3.77 (*s*, 2 CH_2); 3.92, (*s*, 2 CH_2). ^{13}C-NMR (75 MHz, $CDCl_3$): 30.9 (CH_2); 32.9 (C); 33.3 (CH_2); 38.7 (CH_2); 41.6 (CH_2); 50.5 (CH_2); 63.2 (CH_2); 63.3 (CH_2); 96.5 (C); 165.3 (C). HR-ESI-MS: 487.2028 ([M + Na]$^+$, $C_{19}H_{28}N_8{}^{23}NaO_6^+$; calc. 487.2024).

Benzyl 4-[(2,2-Dimethylpropanoyl)oxy]piperidine-1-carboxylate (**9**). Compound **8** [2a] (4.5 g, 19.5 mmol) was dissolved in 100 ml of dry CH_2Cl_2, and 3.2 ml (33.15 mmol, 1.7 equiv.) of pyridine were added (*Scheme 3*). The mixture was cooled to −20°, and 4.0 ml (33.15 mmol, 1.7 equiv.) of pivaloyl chloride (^{t}BuCOCl) were added slowly. The mixture was warmed to r.t. and stirred overnight. The mixture was washed with aq. tartaric acid and sat. aq. $NaHCO_3$ soln. The org. layer was dried ($MgSO_4$), filtered, and evaporated. The resulting residue was purified by FC (CH_2Cl_2/MeOH 100:1) to give **10** (4.5 g, 14.09 mmol, 72%). White solid. R_f (CH_2Cl_2/MeOH 100:1) 0.21. ^{1}H-NMR (300 MHz, $CDCl_3$): 1.20 (*s*, 3 Me); 1.58–1.70 (*m*, CH_2); 1.78–1.90 (*m*, CH_2); 3.46 (*m*, CH_2); 3.62–3.70 (*m*, CH_2); 4.94 (*tt*, J = 7.2, CH); 5.13 (*s*, CH_2); 7.30–7.37 (*m*, 5 arom. H). ^{13}C-NMR (75 MHz, $CDCl_3$): 27.0 (Me); 30.2 (CH_2); 38.7 (C); 40.8 (CH_2); 67.0 (CH_2); 68.5 (CH); 127.8 (arom. C); 127.9 (arom. C); 128.4 (arom. C); 136.6 (arom. C); 155.1 (C); 177.6 (C).

Scheme 3. *Synthesis of Compound* **11**

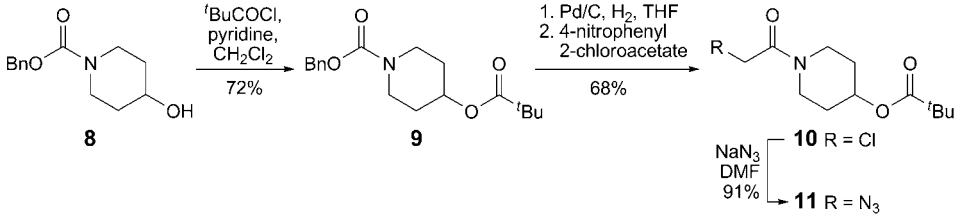

1-(Chloroacetyl)piperidin-4-yl 2,2-Dimethylpropanoate (**10**). Compound **9** (4 g, 11.8 mmol) was dissolved in 100 ml of dry THF. Pd/C (200 mg, 10%) was added, and the suspension was stirred under H_2, until TLC showed complete conversion (*Scheme 3*). The H_2 atmosphere was changed to a N_2 atmosphere, and the mixture was cooled to 0°. 4-Nitrophenyl 2-chloroacetate (2.8 g, 13.06 mmol, 1.1 equiv.) [17] was added. The mixture was warmed to r.t. and stirred for another 12 h. The mixture was filtered through *Celite*, and the solvent was evaporated. The residue was purified by FC (hexane/AcOEt 5:1) to afford **10** (2.1 g, 8.04 mmol, 68%). White solid. R_f (hexane/AcOEt 5:1) 0.36. ^{1}H-NMR (300 MHz, $CDCl_3$): 1.12 (*s*, 3 Me); 1.56–1.91 (*m*, 2 CH_2); 3.36–3.64 (*m*, 2 CH_2); 4.01 (*s*, CH_2); 4.91 (*tt*, J = 3.6, 6.9, CH). ^{13}C-NMR (75 MHz, $CDCl_3$): 26.9 (Me); 29.7 (CH_2); 30.5 (CH_2); 38.5 (C); 38.9 (CH_2); 40.8 (CH_2); 42.9 (CH_2); 67.8 (CH); 164.7 (C); 177.3 (C).

1-(Azidoacetyl)piperidin-4-yl 2,2-Dimethylpropanoate (**11**). To a suspension of **10** (1.75 g, 6.7 mmol) in 20 ml of dry DMF were added 522.6 mg (8.0 mmol, 1.2 equiv.) of NaN_3 (*Scheme 3*). The mixture was stirred for 5 h. Brine (5 ml) was added, and the org. layer was separated. The aq. layer was extracted with 10 ml of CH_2Cl_2, and the combined org. layers were dried ($MgSO_4$). The solvent was removed *in vacuo*. The residue was purified by FC (CH_2Cl_2/MeOH 100:1) to furnish **11** (1.63 g, 6.07 mmol, 91%). White solid. R_f (CH_2Cl_2/MeOH 100:1) 0.29. ^{1}H-NMR (300 MHz, $CDCl_3$): 1.17 (*s*, 3 Me); 1.62–1.91 (*m*, 2 CH_2); 3.25–3.52 (*m*, CH_2); 3.58–3.73 (*m*, CH_2); 3.92 (*s*, CH_2); 4.96 (*tt*, J = 3.6, 6.9, CH). ^{13}C-NMR (75 MHz, $CDCl_3$): 27.0 (Me); 29.9 (CH_2); 30.7 (CH_2); 38.7 (C); 38.9 (CH_2); 41.9 (CH_2); 50.6 (CH_2); 67.9 (CH); 165.4 (C); 177.4 (C).

Synthesis of Fluorescent Dyes. For the [3 + 2] cycloaddition ('click' reaction), fluorescent molecules bearing C≡C bonds without any spacers have been synthesized in good yields (*Scheme 4*).

Scheme 4. *Synthesis of Compounds* **2b** *and* **2c**

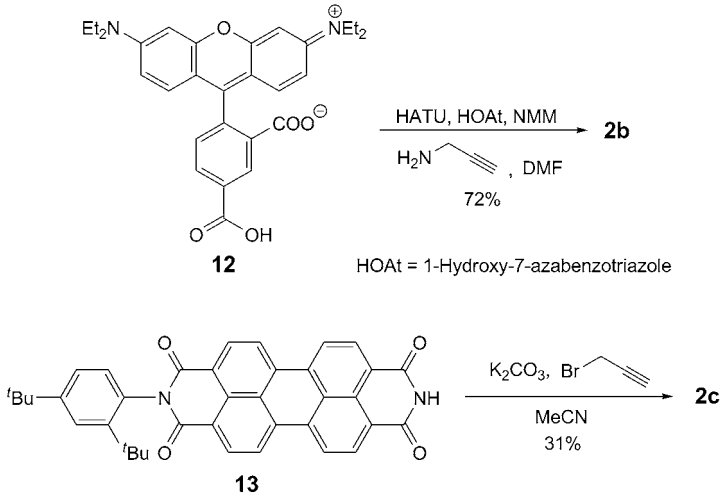

*2-[6-(Diethylamino)-3-(diethyliminio)-3*H*-xanthen-9-yl]-5-(prop-2-yn-1-ylcarbamoyl)benzoate* (**2b**). *5-Carboxytetraethylrhodamine* (**12**; 150 mg, 0.31 mmol) was dissolved in anh. DMF (5 ml), and propargylamine (25 mg, 0.46 mmol, 1.5 equiv.), 2-(7-aza-1*H*-benzotriazole-1-yl)-1,1,3,3-tetramethyluronium hexafluorophosphate (HATU; (243 mg, 0.62 mmol, 2 equiv.), 1-hydroxy-7-azabenzotriazole (HOAt; 84 mg, 0.62 mmol, 2 equiv.) and *N*-methylmorpholine (NMM; 125 mg, 1.23 mmol, 4 equiv.) were added to the soln. After stirring for 24 h at r.t., the solvent was removed *via* rotary evaporation *in vacuo*. The crude product was dried under high vaccum for 2 h. FC (CH_2Cl_2/MeOH/Et_3N 20:1:0.5) afforded **2b** (117 mg, 0.22 mmol, 72%). Dark-pink solid. R_f (CH_2Cl_2/MeOH/Et_3N 10:1:0.5) 0.32. ^{1}H-NMR (500 MHz; $CDCl_3$): 1.30 (*t*, *J* = 8.7, 4 Me); 2.25 (*t*, *J* = 2.47, CH); 3.56 (*q*, *J* = 7.18, 4 CH_2); 4.28 (*dd*, *J* = 2.4, 5.0, CH_2N); 6.70 (*d*, *J* = 2.4, 2 CH); 6.78 (*dd*, *J* = 2.4, 9.5, 2 CH); 7.30 (*d*, *J* = 9.5, 2 CH); 8.15 (*t*, *J* = 5.0, NH); 8.28 (*dd*, *J* = 1.1, 7.9, CH); 8.71 (*s*, CH). ^{13}C-NMR (125 MHz, $CDCl_3$): 12.5 (Me); 29.8 (CH_2N); 45.9 (NCH_2Me); 71.4 (C); 79.3 (C); 96.1 (CH); 113.6 (C); 114.0 (CH); 129.8 (CH); 130.0 (CH); 131.5 (CH); 131.6 (CH); 131.7 (CH); 135.9 (C); 136.1 (C); 155.5 (C); 157.8 (C); 159.3 (CO); 166.0 (C). HR-ESI-MS: 524.2562 ($[M+H]^+$, $C_{32}H_{34}N_3O_4^+$; calc. 524.2549).

*2-[2,4-Di-(*tert*-butyl)phenyl]-9-(prop-2-yn-1-yl)isoquinolino[4',5',6':6,5,10]anthra[2,1,9-*def*]isoquinoline-1,3,8,10(2*H*,9*H*)-tetrone* (**2c**). To a flask containing **13** (167 mg, 0.28 mmol) was added MeCN (5 ml), followed by propargyl bromide (137 mg, 1.15 mmol, 4 equiv.) and K_2CO_3 (399 mg, 2.89 mmol, 10 equiv.), and the suspension was stirred at 85° overnight. The mixture was filtered and concentrated *in vacuo*. The crude product was purified by FC (CH_2Cl_2) to yield **2c** (55 mg, 0.089 mmol; 31%). Purple solid. R_f (CH_2Cl_2) 0.32. ^{1}H-NMR (300 MHz, $CDCl_3$): 1.28 (*s*, ^{t}Bu); 1.38 (*s*, ^{t}Bu); 2.21 (*t*, *J* = 2.4, CH); 4.97 (*d*, *J* = 2.4, CH_2N); 7.28 (*d*, *J* = 2.1, CH); 7.49 (*dd*, *J* = 2.1, 8.6, CH); 7.61 (*d*, *J* = 8.6, CH); 8.54 (*m*, 8 H). HR-ESI-MS: 616.2368 ($[M+H]^+$, $C_{41}H_{32}N_2O_4^+$; calc. 616.2362).

General Procedure 1 (*GP 1*)*: Preparation of Single-Labeled Rods* **3a**–**3d***, and Reference Compounds* **3e** *and* **3f**. The disazido rods **1a**, **1b**, or compound **11**, fluorescent dye **2a** or **2b** (1.1 equiv.), and Et_3N (1.1 equiv.) were dissolved in CH_2Cl_2 (0.5M), and Cu/C (5 mol-%) was added. After stirring overnight, the mixture was diluted with CH_2Cl_2, filtered over *Celite*, and the solvent was evaporated. The resulting residue was purified by FC or semi-prep. RP-HPLC.

General Procedure 2 (*GP 2*)*: Preparation of Double-Labeled Rods* **4c** *and* **4d**. As described in *GP 1*, a soln. of **1a** or **1b**, both fluorescent dyes **2c** and **2d** simultaneously (each 1.1 equiv.), Et_3N (2.2 equiv.), and Cu/C (10 mol-%) was stirred in CH_2Cl_2 (0.5M) at r.t. After 7 h, the mixture was diluted with CH_2Cl_2, filtered over *Celite*, and the solvent was evaporated. The resulting residue was purified by prep. NP-HPLC.

*5-{[(1-{2-[15-(Azidoacetyl)-7,11,18,21-tetraoxa-3,15-diazatrispiro[5.2.2.5^{12}.2^{9}.2^{6}]henicos-3-yl]-2-oxoethyl}-1*H*-1,2,3-triazol-4-yl)methyl]carbamoyl}-2-(6-hydroxy-3-oxo-3*H*-xanthen-9-yl)benzoic Acid* (**3a**). Compound **3a** was synthesized according to *GP 1* with MeOH as solvent instead of CH_2Cl_2. The residue was separated by semi-prep. RP-HPLC, to give **3a** (63%). Yellow solid. RP-HPLC: t_R 12.5 min. MALDI-TOF-MS: 875.81 ($[M+H]^+$, $C_{43}H_{44}N_9O_{12}^+$; calc. 873.31).

*5-{[(1-{2-[15-(Azidoacetyl)-7,11,18,21-tetraoxa-3,15-diazatrispiro[5.2.2.5^{12}.2^{9}.2^{6}]henicos-3-yl]-2-oxoethyl}-1*H*-1,2,3-triazol-4-yl)methyl]carbamoyl}-2-[6-(diethylamino)-3-(diethyliminio)-3*H*-xanthen-9-yl]-benzoate* (**3b**). Compound **3b** was synthesized according to *GP 1*. The residue was separated by semi-prep. RP-HPLC, to give **3b** (74%). Pink solid. RP-HPLC: t_R 14.5 min. MALDI-TOF-MS: 988.26 ($[M+H]^+$, $C_{51}H_{62}N_{11}O_{10}^+$; calc. 988.47).

*5-{[(1-{2-[1′′′′′′′′-(Azidoacetyl)-4′′′′,8′′′′-dibutyl-1*H*-octaspiro[piperidine-4,2′-[1,3]dioxane-5′,5′′-[1,3]dioxane-2′′,1′′′-cyclohexane-4′′′,2′′′′-[1,3]dioxolo[4,5-f][1,3]benzodioxole-6′′′′,1′′′′′-cyclohexane-4′′′′′,2′′′′′-[1,3]dioxane-5′′′′′,5′′′′′′-[1,3]dioxane-2′′′′′′,4′′′′′′-piperidin]-1-yl]-2-oxoethyl}-1*H*-1,2,3-triazol-4-yl)methyl]carbamoyl}-2-(6-hydroxy-3-oxo-3*H*-xanthen-9-yl)benzoic acid* (**3c**). The Compound **3c** was synthesized according to *GP 1* with MeOH/CH_2Cl_2 1:1 as solvent. The yellow residue was purified by semi-prep. RP-HPLC to give **3c** (52%). RP-HPLC: t_R 26.8 min. MALDI-TOF-MS: 1421.53 ($[M+H]^+$, $C_{74}H_{86}N_9O_{20}^+$; calc. 1420.60).

*5-{[(1-{2-[1′′′′′′′′-(Azidoacetyl)-4′′′′,8′′′′-dibutyl-1*H*-octaspiro[piperidine-4,2′-[1,3]dioxane-5′,5′′-[1,3]dioxane-2′′,1′′′-cyclohexane-4′′′,2′′′′-[1,3]dioxolo[4,5-f][1,3]benzodioxole-6′′′′,1′′′′′-cyclohexane-4′′′′′,2′′′′′-[1,3]dioxane-5′′′′′,5′′′′′′-[1,3]dioxane-2′′′′′′,4′′′′′′-piperidin]-1-yl]-2-oxoethyl}-1*H*-1,2,3-triazol-4-yl)methyl]carbamoyl}-2-[6-(diethylamino)-3-(diethyliminio)-3*H*-xanthen-9-yl]benzoate* (**3d**). Compound **3d** was synthesized according to *GP 1*. The resulting residue was purified by FC (CH_2Cl_2/MeOH/Et_3N 20:1:0.5) to give **3d** (65%). Pink solid. R_f (CH_2Cl_2/MeOH/Et_3N 20:1:0.5) 0.18. MALDI-TOF-MS: 1531.52 ($[M+H]^+$, $C_{82}H_{104}N_{11}O_8^+$; calc. 1530.76).

*5-({[1-(2-{4-[(2,2-Dimethylpropanoyl)oxy]piperidin-1-yl}-2-oxoethyl)-1*H*-1,2,3-triazol-4-yl]methyl}-carbamoyl)-2-(6-hydroxy-3-oxo-3*H*-xanthen-9-yl)benzoic Acid* (**3e**). Compound **3e** was synthesized according to *GP 1* with MeOH as solvent instead of CH_2Cl_2. The residue was purified on a *Sephadex LH 20* column with MeOH and yielded **3e** (63%). Yellow solid. R_f (CH_2Cl_2/MeOH 100:5) 0.38. MALDI-TOF-MS: 706.37 ($[M+Na]^+$, $C_{36}H_{35}N_5{}^{23}NaO_9^+$; calc. 704.23).

*2-[6-(Diethylamino)-3-(diethyliminio)-3*H*-xanthen-9-yl]-5-({[1-(2-{4-[(2,2-dimethylpropanoyl)-oxy]piperidin-1-yl}-2-oxoethyl)-1*H*-1,2,3-triazol-4-yl]methyl}carbamoyl)benzoate* (**3f**). Compound **3f** was synthesized as described for **3e**. The residue was separated by using a *Sephadex LH 20* column to give **3f** (53%). Purple solid. R_f (CH_2Cl_2/MeOH 10:1) 0.42. MALDI-TOF-MS: 794.36 ($[M+H]^+$, $C_{44}H_{54}N_7O_9^+$; calc. 792.41).

*5-[({1-[2-(15-{[4-({[3-Carboxy-4-(6-hydroxy-3-oxo-3*H*-xanthen-9-yl)benzoyl]amino}methyl)-1*H*-1,2,3-triazol-1-yl]acetyl}-7,11,18,21-tetraoxa-3,15-diazatrispiro[5.2.2.5^{12}.2^{9}.2^{6}]henicos-3-yl)-2-oxoethyl]-1*H*-1,2,3-triazol-4-yl}methyl)carbamoyl]-2-[6-(diethylamino)-3-(diethyliminio)-3*H*-xanthen-9-yl]benzoate* (**4a**). A suspension of **3b** (5 mg, 5.06 μmol, 1 equiv.), **2a** (2.3 mg, 5.57 μmol, 1.1 equiv.), Et_3N (0.8 μl, 5.57 μmol, 1.1 equiv.) and 1 mg of Cu/C was stirred in MeOH (150 μl) at r.t., and the reaction was monitored by TLC. After 7 h, the mixture was diluted with MeOH, filtered over *Celite*, and the solvent was evaporated. The purple residue was purified by semi-prep. RP-HPLC to give **4a** (2.8 mg, 2.0 μmol, 39%). t_R 13.4 min. MALDI-TOF-MS: 1402.09 ($[M+H]^+$, $C_{75}H_{77}N_{12}O_{16}^+$; calc. 1401.56).

*5-[({1-[2-(4′′′′,8′′′′-Dibutyl-1′′′′′′′′-{[4-({[3-carboxy-4-(6-hydroxy-3-oxo-3*H*-xanthen-9-yl)benzoyl]-amino}methyl)-1*H*-1,2,3-triazol-1-yl]acetyl}-1*H*-octaspiro[piperidine-4,2′-[1,3]dioxane-5′,5′′-[1,3]dioxane-2′′,1′′′-cyclohexane-4′′′,2′′′′-[1,3]dioxolo[4,5-f][1,3]benzodioxole-6′′′′,1′′′′′-cyclohexane-4′′′′′,2′′′′′-[1,3]dioxane-5′′′′′,5′′′′′′-[1,3]dioxane-2′′′′′′,4′′′′′′-piperidin]-1-yl)-2-oxoethyl]-1*H*-1,2,3-triazol-4-yl}methyl)carbamoyl]-2-[6-(diethylamino)-3-(diethyliminio)-3*H*-xanthen-9-yl]benzoate* (**4b**). A suspension of **3d** (3.6 mg, 2.35 μmol, 1 equiv.), **2a** (1.1 mg, 2.59 μmol, 1.1 equiv.), Et_3N (0.4 μl, 2.59 μmol, 1.1 equiv.)

and 1 mg of Cu/C was stirred in CH_2Cl_2/MeOH 1:1 (200 µl) at r.t., and the reaction was monitored by TLC. After 8 h, the mixture was diluted with CH_2Cl_2 and filtered over *Celite*. The solvent was evaporated, and the resulting residue was purified by size exclusion chromatography (*Sephadex LH 20*; CH_2Cl_2/MeOH 1:1) to yield **4b** (2.5 mg, 1.29 µmol, 55%). Purple solid. MALDI-TOF-MS: 1944.41 ($[M+H]^+$, $C_{106}H_{119}N_{12}O_{24}$; calc. 1943.85).

*2-[2,4-Di-(*tert*)-butylphenyl]-9-[(1-{2-oxo-2-[15-({4-[(pyren-1-ylmethoxy)methyl]-1*H*-1,2,3-triazol-1-yl}acetyl)-7,11,18,21-tetraoxa-3,15-diazatrispiro[5.2.2.5*^{12}*.2*^{9}*.2*^{6}*]henicos-3-yl]ethyl}-1*H*-1,2,3-triazol-4-yl)methyl]isoquinolino[4′,5′,6′:6,5,10]anthra[2,1,9-*def*]isoquinoline-1,3,8,10(2*H*,9*H*)-tetrone* (**4c**). Compound **4c** was synthesized according *GP 2*, by simultaneous 'click' reaction of **1a**, and fluorescent dyes **2c** and **2d**. NP-HPLC (CH_2Cl_2/MeOH 100:5) afforded **4c** (38%). Purple solid. t_R 7.8 min. MALDI-TOF-MS: 1352.25 ($[M+H]^+$, $C_{80}H_{75}N_{10}O_{11}$; calc. 1351.56), 1375.23 ($[M+Na]^+$, $C_{85}H_{74}N_{10}{}^{23}NaO_{11}^+$; calc. 1373.54).

*2-(2,4-Di-(*tert*)-butylphenyl)-9-[(1-{2-[4‴,8‴‴-dibutyl-1‴‴‴‴‴-({4-[(pyren-1-ylmethoxy)methyl]-1*H*-1,2,3-triazol-1-yl}acetyl)-1*H*-octaspiro[piperidine-4,2′-[1,3]dioxane-5′,5″-[1,3]dioxane-2″,1‴-cyclohexane-4‴,2‴‴-[1,3]dioxolo[4,5-f][1,3]benzodioxole-6‴‴,1‴‴‴-cyclohexane-4‴‴‴,2‴‴‴‴-[1,3]dioxane-5‴‴‴‴,5‴‴‴‴‴-[1,3]dioxane-2‴‴‴‴‴,4‴‴‴‴‴-piperidin]-1-yl]-2-oxoethyl}-1*H*-1,2,3-triazol-4-yl)methyl]isoquinolino[4′,5′,6′:6,5,10]anthra[2,1,9-*def*]isoquinoline-1,3,8,10(2*H*,9*H*)-tetrone* (**4d**). Compound **4d** was synthesized according to *GP 2*, by simultaneous 'click' reaction of **1b** and fluorescent dyes **2c** and **2d** . The resulting residue was purified by NP-HPLC ($CHCl_3$/^{i}PrOH 100:4) to afford **4d** (32%). Purple solid. t_R 6.5 min. MALDI-TOF-MS: 1895.27 ($[M+H]^+$, $C_{111}H_{117}N_{10}O_{19}^+$; calc. 1893.85), 1917.38 ($[M+Na]^+$, $C_{111}H_{116}N_{10}{}^{23}NaO_{19}^+$; calc. 1915.83).

Absorption and Steady-State Fluorescence Spectroscopy. The absorption spectra were recorded with a *Cary 500* UV/VIS spectrometer (*Varian*, DE-Darmstadt) in the spectral range of $400\text{ nm} < \lambda_{abs} < 700\text{ nm}$, and the background-corrected steady-state fluorescence spectra were recorded on a *Fluoromax-3* spectrofluorometer (*HORIBA Jobin Yvon GmbH*, DE-Munich). The fluorescence quantum yields were determined on a quantum yield fluorescence spectrometer using an integrating sphere (*PL Quantum Yield Measurement System C9920-02*, *Hamamatsu Photonics*, Japan).

Time-Resolved Fluorescence Spectroscopy and Depolarization Measurements. The fluorescence-decay times were determined with a *FLS920* fluorescence lifetime spectrophotometer (*Edinburgh Instruments*, UK-Livingston) operated in the time-correlated single photon-counting (TCSPC) mode. Samples were excited with a vertically polarized supercontinuum white light source (*SC400-PP*, *Fianium Ltd.*, UK-Southhampton) at a repetition rate of 20 MHz and a pulse width (FWHM) of 30 ps. For the detection under magic angle conditions (54.8°), a multichannel plate (*ELDY EM1-132/300 MCP-PMT*, *Europhoton*, DE-Berlin) was used (see *Table 1* for specific information on excitation and emission wavelengths).

For the determination of the time-resolved anisotropy (including the respective G factor), the fluorescence-decay curves were recorded with an emission polarizer placed in vertical and horizontal position, resp. The experimental data were evaluated using *Eqns. 2* and *3* [18a]:

$$r(t) = \frac{I_{vv}(t) - I_{vh}(t) \cdot G}{I_{vv}(t) + 2 \cdot I_{vh}(t) \cdot G} \tag{2}$$

$$G = \frac{I_{hv}}{I_{hh}} \tag{3}$$

For small molecules, the anisotropy decay, $r(t)$, can be analyzed according to *Eqn. 4* [18a]:

$$r(t) = r_0 \cdot exp\left(-\frac{t}{\phi}\right) \tag{4}$$

From the evaluation of $r(t)$, the fundamental anisotropy, r_0, at the time $t=0$, and the rotational correlation time φ of the molecule were obtained. The fundamental anisotropy, r_0, was also determined in a reference experiment measuring the steady-state anisotropy at 77 K.

For the analysis of the fluorescence-anisotropy data obtained for micellar samples, the 'two-step' model as an extension of the 'wobbling-in-cone' model was applied [18b]. For dyes incorporated in micelles, two motions causing depolarization are considered: *i*) a fast hindered rotation of the dye molecules within the micellar environment, resulting in an anisotropy loss, and *ii*) a contribution of the slow overall motion of the micelle itself. In such a case, the time-resolved anisotropy is a product of the two anisotropy functions describing the different motions (see *Eqn. 5*) [18b]:

$$r(t) = r_{fast}(t) \cdot r_{slow}(t) = \left(1 - S^2\right) \cdot exp\left(\frac{-t}{\phi_{fast}}\right) + S^2 exp\left(\frac{-t}{\phi_{slow}}\right) \tag{5}$$

with φ_{slow} and φ_{fast} describing the rotational correlation time of the slow and fast motion, resp. Here, the slow rotational correlation time, φ_{slow}, is a sum of the rotational motion of the micelle (φ_M) and the lateral diffusion of the dye in the micelle (φ_L) [18b]:

$$\frac{1}{\phi_{slow}} = \frac{1}{\phi_M} + \frac{1}{\phi_L} \tag{6}$$

The fast correlation time φ_{fast} is defined according to [18b]:

$$\frac{1}{\phi_{fast}} = \frac{1}{\phi_w} + \frac{1}{\phi_{slow}} \tag{7}$$

with the effective correlation time φ_w (reorientation time for the wobbling motion).

The relationship between the anisotropy decay, $r(t)$, and the structure of the micelles can be followed using the order parameter *S*. In case the motion is fast and isotropic, $S = 0$, and in case the motion is completely restricted, $S = 1$. The simple 'wobbling-in-cone' model describes a restricted motion for a symmetrical ellipsoid with its transition dipole moment parallel to the symmetry axis and the molecule diffusing freely in a cone with an angle θ. The wobbling cone angle θ can be calculated using *S* [18b]:

$$S^2 = \left[\frac{1}{2} \cdot (cos\theta) \cdot (1 + cos\theta)\right]^2 \text{ for } 0 \leq \theta \leq 90^\circ \tag{8}$$

For the analysis, the weighting w_i of the anisotropy data was carried out according to *Eqn. 9* [18c]:

$$w_i = \frac{3 \cdot [I_{vv}(t_i) + 2 \cdot I_{vh}(t_i)]}{2 + r(t_i) + 5 \cdot [r(t_i)]^2 - 2 \cdot [r(t_i)]^3} \quad \text{with } i = 1...2 \tag{9}$$

Single-Molecule Fluorescence Measurements. Single-molecule fluorescence experiments were performed on an inverse time-resolved fluorescence confocal microscope system *MicroTime 200* driven by a *PicoHarp 300* PC-board (*PicoQuant*, DE-Berlin). Excitation at λ_{exc} 470 nm was carried out with a supercontinuum white light source (*SC400-2*, *Fianium Ltd.*, UK-Southhampton) operated at a repetition rate of 20 MHz. The excitation light was coupled *via* a single mode fibre into the body of the inverted microscope (*Olympus IX71*). The excitation power of (70 ± 5) μW was measured at the focus of the microscope objective. The data were collected for 20 min at $T = (294 \pm 1)$ K. After reflection by a dichroic mirror, the collimated laser beam was focused by an oil immersion objective (*Olympus*, *PlanApo*, 100x/NA1.4). The collected fluorescence light was transmitted by the dichroic mirror, passed a long-pass 500-nm filter for complete excitation light rejection and a 50-μm pinhole. To distinguish between the donor and acceptor emission, a band-pass filter of 522 nm (*BP 522/15*, *Semrock*, *Inc.*, USA) and of 589 nm (*BP 589/15*, *Semrock, Inc.*, USA) was placed in front of the avalanche photodiodes (*SPCM-AQR-13 & SPCM-CD-2801*, *Perkin-Elmer*, Waltham, USA), resp. The signals of the donor and acceptor channel were separately but simultaneously detected as a function of time and binned in 1-ms time intervals. After removing the background noise by setting a threshold to filter out the significant bursts of photons, the FRET efficiency was calculated according to *Eqn. 10*, using the software SymPhoTime 5.1.31 (*PicoQuant*, DE-Berlin) [19][20]:

$$E = \frac{n_A - n_D \cdot L_{AD}}{n_A \cdot (1 - L_{DA}) + n_D \cdot (\gamma - L_{AD})} \tag{10}$$

In *Eqn. 10*, n_A and n_D denote the number of photons in the burst of the acceptor and donor channel, resp., γ is the compensation for the quantum yields of the dyes and detection efficiency differences between donor and acceptor channel. Due to the difficulties in the determination of the experimental parameter, γ was assumed to be 1 [19]. Compensation for the donor/acceptor and acceptor/donor bleed through, L_{DA} and L_{AD}, was experimentally determined with the single dye-labeled samples. No photobleaching of the dyes was observed during the experiments.

Ensemble FRET Experiments. In ensemble measurements, the FRET efficiencies were calculated from the fluorescence intensities and decay times of the donor in the absence (I_D and τ_D) and presence (I_{DA} and τ_{DA}) of acceptor molecules according to *Eqn. 11* [18a]:

$$E^E = 1 - \frac{I_{DA}}{I_D} and E^\tau = 1 - \frac{\tau_{DA}}{\tau_D} \tag{11}$$

The calculated FRET efficiency (E^C) was derived from [18a]:

$$E^C = \frac{R_0^6}{R_0^6 + R^6} \tag{12}$$

with the interchromophoric distance R, and the critical *Förster* distance R_0 that was calculated according to *Eqn. 13* [21]:

$$R_0^6 = \frac{9 \cdot \ln(10) \cdot \kappa^2 \cdot \Phi_{F,D}}{128 \cdot \pi^5 \cdot N_A \cdot n^4} \cdot \int_0^\infty I_D(\lambda) \cdot \varepsilon_A(\lambda) \cdot \lambda^4 \cdot d\lambda \tag{13}$$

In *Eqn. 13*, the *Avogadro* constant is given by N_A and the refractive index by n. The orientation factor is denoted by κ^2, and the quantum yield of the donor in the absence of energy transfer is $\Phi_{F,D}$. The spectral overlap integral J was calculated from the normalized fluorescence spectrum of the donor $I_D(\lambda)$ and the molar absorption coefficient $\varepsilon_A(\lambda)$ of the acceptor.

REFERENCES

[1] a) D. M. Togashi, B. Szczupak, A. G. Ryder, A. Calvet, M. O'Loughlin, *J. Phys. Chem. A* **2009**, *113*, 2757; b) N. Marmé, J.-P. Knemeyer, M. Sauer, J. Wolfrum, *Bioconjugate Chem.* **2003**, *14*, 1133; c) X. Li, R. Zhu, A. Yu, X. S. Zhao, *J. Phys. Chem. B* **2011**, *115*, 6265; d) J. R. Unruh, G. Gokulrangan, G. H. Lushington, C. K. Johnson, G. S. Wilson, *Biophys. J.* **2005**, *88*, 3455; e) E. Dolghih, A. E. Roitberg, J. L. Krause, *J. Photochem. Photobiol., A* **2007**, *190*, 321; f) A. Iqbal, S. Arslan, B. Okumus, T. J. Wilson, G. Giraud, D. G. Norman, T. Ha, D. M. J. Lilley, *Proc. Natl. Acad. Sci. U.S.A.* **2008**, *105*, 11176.

[2] a) P. Wessig, K. Möllnitz, C. Eiserbeck, *Chem. – Eur. J.* **2007**, *13*, 4859; b) P. Wessig, K. Möllnitz, *J. Org. Chem.* **2008**, *73*, 4452; c) P. Müller, J. Nikolaus, S. Schiller, A. Herrmann, K. Möllnitz, S. Czapla, P. Wessig, *Angew. Chem.* **2009**, *121*, 4497; d) J. Nikolaus, S. Czapla, K. Möllnitz, C. T. Höfer, A. Herrmann, P. Wessig, P. Müller, *Biochim. Biophys. Acta, Biomembr.* **2011**, *1808*, 2781; e) P. F. H. Schwab, M. D. Levin, J. Michl, *Chem. Rev.* **1999**, *99*, 1863.

[3] a) M. Sauer, K. H. Drexhage, U. Lieberwirth, R. Müller, S. Nord, C. Zander, *Chem. Phys. Lett.* **1998**, *284*, 153; b) M. Sauer, K.-T. Han, R. Müller, S. Nord, A. Schulz, S. Seeger, J. Wolfrum, J. Arden-Jacob, G. Deltau, N. J. Marx, C. Zander, K. H. Drexhage, *J. Fluoresc.* **1995**, *5*, 247; c) F. F. Lewis, T. Wu, Y. Zhang, R. L. Letsinger, S. R. Greenfield, M. R. Wasielewski, *Science* **1997**, *277*, 673; d) A. Dietrich, V. Buschmann, C. Müller, M. Sauer, *Rev. Mol. Biotechnol.* **2002**, *82*, 211.

[4] D. Bose, D. Sarkar, N. Chattopadhyay, *Photochem. Photobiol.* **2010**, *86*, 538; M. E. Sanborn, B. K. Connolly, K. Gurunathan, M. Levitus, *J. Phys. Chem. B* **2007**, *111*, 11064; G. Vámosi, C. Gohike, R. M. Clegg, *Biophys. J.* **1996**, *71*, 972.
[5] P. Wu, V. V. Fokin, *Aldrichim. Acta* **2007**, *40*, 7; H. C. Kolb, H. G. Finn, K. B. Sharpless, *Angew. Chem.* **2001**, *113*, 2056; *Angew. Chem., Int. Ed.* **2001**, *40*, 2004; M. G. Finn, V. V. Fokin, *Chem. Soc. Rev.* **2010**, *39*, 1231.
[6] B. H. Lipshutz, B. R. Taft, *Angew. Chem., Int. Ed.* **2006**, *45*, 8235.
[7] a) M. Dominska, G. J. Blanchard, *Langmuir* **2010**, *26*, 1043; b) L. You, G. W. Gokel, *Chem. – Eur. J.* **2008**, *14*, 5861; c) C. E. Bunker, B. Ma, K. J. Simmons, H. W. Rollins, J. T. Liu, J. J. Ma, C. W. Martin, D. D. DesMarteau, Y. P. Sun, *J. Electroanal. Chem.* **1998**, *459*, 15; d) E. Szajdzinska-Pietek, M. Wolszczak, A. Plonka, S. Schlick, *J. Am. Chem. Soc.* **1998**, *120*, 4215.
[8] S. Voss, R. Fischer, G. Jung, K.-H. Wiesmueller, R. Brock, *J. Am. Chem. Soc.* **2007**, *129*, 554; F. Caruso, E. Donath, H. Mohwald, *J. Phys. Chem. B* **1998**, *102*, 2011; T. Tuschl, C. Gohlke, T. M. Jovin, E. Westhof, F. Eckstein, *Science* **1994**, *266*, 785.
[9] R. F. Chen, J. R. Knutson, *Anal. Biochem.* **1988**, *172*, 61.
[10] D. A. Holowka, B. Baird, *Biochemistry* **1983**, *22*, 3466.
[11] I. Z. Steinberg, *J. Chem. Phys.* **1968**, *48*, 2411.
[12] Y. O. Posokhov, M. Merzlyakov, K. Hristova, A. S. Ladokhin, *Anal. Biochem.* **2008**, *380*, 134.
[13] B. A. Coles, R. G. Compton, *J. Electroanal. Chem.* **1983**, *144*, 87.
[14] Y. Hua, A. H. Flood, *Chem. Soc. Rev.* **2010**, *39*, 1262.
[15] A. Techen, C. Hille, C. Dosche, M. U. Kumke, *J. Colloid Interface Sci.* **2012**, *377*, 251.
[16] N. C. Maiti, M. M. G. Krishna, P. J. Britto, N. Periasamy, *J. Phys. Chem.* **1997**, *101*, 11051; G. B. Dutt, *J. Phys. Chem.* **2002**, *106*, 7398.
[17] D. Behar, P. Neta, *J. Phys. Chem.* **1981**, *85*, 690.
[18] a) J. R. Lakowicz, 'Principles of Fluorescence Spectroscopy', 3rd edn., Springer Science + Business Media, New York, 2006; b) E. L. Quitevis, A. H. Marcus, M. D. Fayer, *J. Phys. Chem.* **1993**, *97*, 5762; c) D. V. O'Connor, D. Phillips, 'Time-correlated Single Photon Counting', Academic Press, London, 1984, Chapt. 8.
[19] B. Schuler, E. A. Lipman, W. A. Eaton, *Nature* **2002**, *419*, 743.
[20] M. Dahan, A. A. Deniz, T. Ha, D. S. Chemla, P. G. Schultz, S. Weiss, *Chem. Phys.* **1999**, *247*, 85.
[21] A. Kupstat, T. Ritschel, M. U. Kumke, *Bioconjugate Chem.* **2011**, *22*, 2546.

Received November 21, 2012